symmetry

MDPI

Article

Computational, Investigational Explorations on Structural, Electro-Optic Behavior of Pelargonidin Organic Colorant for TiO_2 Based DSSCs

Satish Kumar Palanisamy [1], Arun Kumar Udayakumar [2], Azher M. Abed [3], Parthasarathy Panchatcharam [4], Suvitha Athisaya Rajah [5], Bradha Madhavan [6,*] and Ananth Steephen [7,*]

1 Department of Mechanical Engineering, Study World College of Engineering, Coimbatore 641105, India
2 Department of Electrical and Electronics Engineering, SRM Institute of Science and Technology, Ramapuram Campus, Chennai 600089, India
3 Department of Air Conditioning and Refrigeration, Al-Mustaqbal University College, Hillah 51001, Iraq
4 Department of Electronics and Communication Engineering, CMR Institute of Technology, Bengaluru 560037, India
5 Department of Physics, CMR Institute of Technology, Bengaluru 560037, India
6 Rathinam Research Centre, Rathinam Technical Campus, Coimbatore 641021, India
7 Department of Physics, KPR Institute of Engineering and Technology, Coimbatore 641407, India
* Correspondence: bradhaaraj@gmail.com (B.M.); ananth.steephen@yahoo.com (A.S.)

Abstract: In an expedition for green-energy generation and to lower the cost per watt of solar energy, environmentally friendly biotic colorants were separated from Tectona grandis seeds. The prime colorant in the extract is pelargonidin which sensitizes titanium dioxide (TiO_2)-based photo anodes. The pelargonidin-sensitized TiO_2 nanomaterials endured structural, photosensitive, spectral and current-voltage interpretations. Frontier molecular orbital analysis, physicochemical and electronic parameter computation, UV–visible and DOS spectral analysis, van der Waals prediction and molecular electrostatic potential map were performed theoretically with Gaussian tools, and IR symmetry response was computed using the crystal maker software package. The pelargonidin-sensitized TiO_2-created dye-sensitized solar cells which exhibited capable solar light energy to photon conversion proficiency. For comparative purposes, the commercial P25 Degussa TiO_2-based DSSC was also fabricated and its proficiency was analyzed. The commercial TiO_2 exhibited 57 % higher proficiency in comparison to the sol-gel-derived TiO_2-based DSSC.

Keywords: pelargonidin dye; symmetry studies; titanium dioxide; dye-sensitized solar cells

Citation: Palanisamy, S.K.; Udayakumar, A.K.; Abed, A.M.; Panchatcharam, P.; Athisaya Rajah, S.; Madhavan, B.; Steephen, A. Computational, Investigational Explorations on Structural, Electro-Optic Behavior of Pelargonidin Organic Colorant for TiO_2 Based DSSCs. *Symmetry* **2023**, *15*, 22. https://doi.org/10.3390/sym15010022

Academic Editors: György Keglevich, Sergei D. Odintsov and Alexey V. Lukoyanov

Received: 31 October 2022
Revised: 3 December 2022
Accepted: 16 December 2022
Published: 22 December 2022

1. Introduction

Energy researchers are exploring abundantly available natural resources in their quest for global clean alternate energy sources with a low carbon footprint. Through the photoelectric effect, solar energy, a prominent renewable energy source, can be harnessed via various solar cells [1–4]. Among these, dye-sensitized solar cells (DSSCs) have a lower cost per watt production cost due to their ease of fabrication, relatively simple method and equipment compatible with mass production, and variety of applications such as wearable devices, indoor photovoltaic windows, and so on [5]. Photosensitizers are essential in DSSCs for capturing solar light photons and generating electric charges [6,7]. Harvesting electrical energy from solar energy will benefit the world to meet growing energy demand. Semiconductor, colorant sensitizer, electrolyte and electrode are all part of it. DSSC efficiency is primarily determined by its components, design, and fabrication processes [8–10]. Because of its obtainability, superior stability, non-toxicity and cost-effectiveness, TiO_2 is a perfect choice for DSSC owing to its size, shape and dimensionality which all have a strong influence on the efficiency of DSSCs. The efficiency of TiO_2-based DSSCs can be boosted by raising their photon absorption [11,12]. The most successful dyes,

such as ruthenium, are synthetic, expensive, difficult to synthesize, multifaceted in design, limited in availability, toxic in nature and pose high environmental risks, among other things [13–15]. In order to generate green energy with a low cost per watt, this research employed an organic photosensitizer extracted from Tectona grandis seeds (pelargonidin). Natural dyes are non-toxic and safe for the environment. Natural dyes have a high potential in the growing demand for eco-friendly coloring agents in process industries such as food, textiles, leather and others. Hence, the high cost, toxic ruthenium chemical dye is eliminated and replaced with pelargonidin dye extracted from Tectona grandis seeds [16,17]. Tectona grandis, generally known for its timber, teak or Sagun, has potential medicinal and pigment value in its seeds, bark, leaves, etc. Pelargonidin, also known as 3,4′,5,7-tetrahydroxy flavylium Pelargonidol chloride, is a multicomponent structure. Its chemical formula is $C_{15}H_{11}O_5$. The major advantage of pelargonidin dye extracted from Tectona grandis seeds is the greater pigment presence than in other parts such as leaves and the seed's lifetime being long. Many reports have recently been published on the use of extracted natural dyes from natural products that have been tested for DSSCs. Prof. Michael Graetzel's research at EPFL has shown the efficiency of DSSCs to be 14.1% with ruthenium-based dyes. As sensitizers in DSSCs, pelargonium and pelargonium grandiflorum achieved efficiencies of 0.065% and 0.067%, respectively. The dye was extracted from the leaves of red amaranth and the effect of different solvents, such as water and ethanol, was studied, yielding PCE values of 0.230% and 0.530%. The dye extracted from Sambucus Ebulus had a PCE of 1.15%. Natural colorant extracted from Butea Monosperma petals exhibited 0.87% efficiency. Lawsonia Inermis seed extract based DSSCs showed 1.0% efficiency. The efficiency of Caesalpinia Sappan heartwood extract sensitized DSSC is 1.1%. In addition, the symmetry of TiO_2′s crystalline structure is critical for tuning surface energy, binding energy, band structure, charge mobility and other parameters that improve the opto-electronic behavior of solar cells [18]. As a result, it is necessary to investigate the interconnectedness of TiO_2 symmetry with the pelargonidin organic colorant to enhance physical and chemical behavior in solar-cell applications [19]. In computational investigations, frontier molecular orbital analysis, physicochemical and electronic parameter calculation, UV–visible and DOS spectral analysis, van der Waals prediction and molecular electrostatic potential map were performed by means of Gaussian tools, and the IR symmetry response was calculated using crystal maker software. The pelargonidin natural photosensitizer extracted from Tectona grandis seeds is used for the first time in DSSCs. This pelargonidin-dye-sensitized TiO_2 has the required properties as a possible future photovoltaic device material and for use in DSSCs, according to the experimental and computational detail investigation.

2. Materials and Methods

As a titanium precursor, Sigma-Aldrich's titanium isopropoxide was employed. The nitric acid, isopropanol and double-distilled water were purchased from Merck. The Tectona grandis seeds were gathered from Coimbatore, Tamilnadu, India.

Tectona grandis, usually known as teak or Sagun, is a strong, tall and high timber-valued tree. Its dry fruits are dark brownish black, spherical-shaped ones and shown in Figure 1a; the pelargonidin dye structure is depicted in Figure 1b.

The Tectona grandis seed extract contains pelargonidin as a major pigment. The fresh, fully matured Tectona grandis seeds were gathered, gutted and dehydrated under shadow for five days to remove the moisture completely. Before using, the outer casing of the Tectona grandis seeds was detached. Seeds were dried at room temperature. The 200 g of Tectona grandis seeds were crushed well and retained in 100 mL ethanol for three days. The blend was filtered by eliminating dense fragments and the filtrate was obtained. The dark-brownish-black-colored aqueous extract of the Tectona grandis seed was utilized as photosensitizer for TiO_2-based DSSCs. Pelargonidin is the key pigment of Tectona grandis seed extract; the optimized molecular structure of pelargonidin (PGN) and van der Waals prediction are depicted in Figure 2a,b.

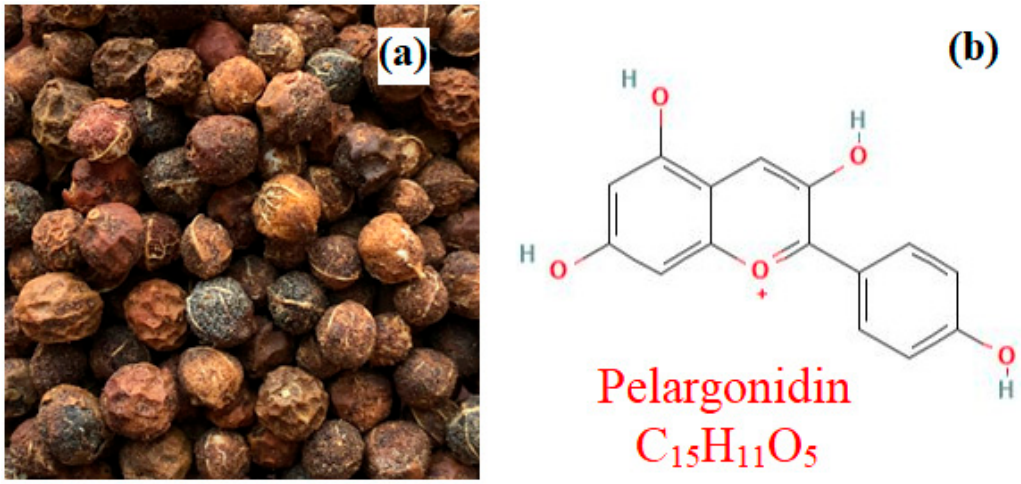

Figure 1. (**a**) Tectona grandis seeds and (**b**) pelargonidin dye structure.

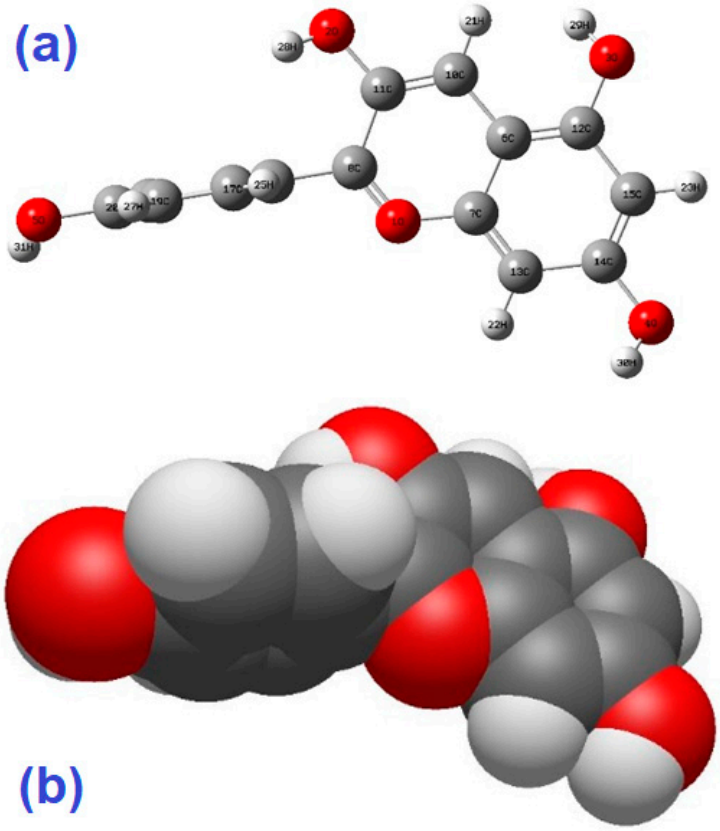

Figure 2. Optimized molecular structure (**a**) and van der Waals prediction of pelargonidin (**b**).

Pure TiO_2 was synthesized by mixing 5 mL of titanium isopropoxide, the titanium precursor, with a combination of 250 mL distilled water and 15 mL isopropanol employing vigorous stirring. The white precipitation which formed was heated at 80 °C for 2 h. It was washed in water and ethanol before drying to obtain pure TiO_2.

2.1. Fabrication of DSSCs

The conducting glass substrate (FTO) with surface resistivity ~13 Ω / sq was cleaned and rinsed with deionized water and then in 2-propanol. Then, it was dried in air prior to film preparation. Scotch tape was used as a mask for the edge area of the TCO which acted as the contact in the final DSSC. The exposed cell area was 0.75 cm^2. The pure

TiO_2 nanoparticles synthesized using sol-gel technique were made into a paste containing titanium isopropoxide. This TiO_2 and titanium isopropoxide solution was mixed and ground well to result in a homogeneous paste. This paste was layered over the FTO plate to form a slim film by employing the doctor-blade technique. In order to form a uniform film, this coating process was repeated. The dried TiO_2-coated FTO glass plate was sintered at 450 °C for 30 min to enhance the electronic contact with TiO_2 and to eradicate inner gas and voids. The TiO_2 photo anode was soaked in 10 mL solution of organic photosensitizer for 12 h to get adsorbed onto its surface in the absence of sunlight. Then, the TiO_2 photoanode was cleansed in ethanol to remove loosely bound natural dye. After that, the working photoanode (TiO_2 + dye) was dehumidified at 25 °C for 30 min. A thin layer of platinum was coated over the FTO glass plate by means of sputtering, serving as the counter electrode. The iodide electrolyte solution was blended by dissolving 0.127 g of iodine (I_2) in 10 mL of ethylene glycol. Then, 0.83 g of potassium iodide (KI) was added to the above solution, stirred and stored in the dark. The triiodide was attained by liquifying 525 milligrams of potassium iodide with 330 milligrams of iodide into 7.5 mL glacial acetic acid. The 0.5 molar alkyl benzimidazole was employed as additive for the electrolyte solution. This solution was stirred in a magnetic stirrer for 30 min to change to a dark-brown triiodide solution. Subsequently, the photoanode and counter electrode were bonded together by crocodile clips without forming air bubbles. The prepared liquid iodide electrolyte combination of KI and I_2 with concentration of 0.6 mol/L and 0.075 mol/L was injected into the inter space carefully. Then, the DSSC was sealed using binder clips and assembled to fabricate TiO_2-based DSSC. By following the same process, commercial P25 Degussa TiO_2-based DSSC was fabricated.

2.2. Computational Information

PGN was calculated using the G09W (M. J. Frisch 2009) and GV5.0.8 (Frisch et al. 2009) applications [20]. In the computations, B3LYP was employed with the 6-311G++ (d, p) set. The optimum geometry, MEP, and IR symmetry response for PGN were calculated. The DOS diagrams were represented using the Gauss Sum [21] program.

A van der Waals complex is a loosely bound complex molecule kept together by intermolecular interactions such as van der Waals forces or hydrogen bonds [22]. Figure 2b shows no van der Waals complex. It demonstrates that the hydrogen bond's potential energy surfaces are closely connected to the other atoms, indicating the absence of van der Waals complex of pelargonidin. SMILE notation of this compound is [H]OC1=C([H]) C([H])=C(C([H])=C1[H]) C1=[O+]C2=C([H]) C(O[H])=C([H]) C(O[H])=C2C([H])=C1O[H].

3. Results and Discussion

3.1. Structural Studies

The PXRD of pure TiO_2 after calcination at 250 °C portrayed in Figure 3 shows the diffraction peaks (101), (004), (200), (211), (204), (116) and (215). This confirms the anatase phase of TiO_2 which possesses better photocatalytic properties than rutile and brookite phases. In addition, the diffraction peaks related to rutile and brookite phases do not exist. The average grain size obtained by Scherrer's equation, $D = K\lambda/(\beta\cos\theta)$, is approximately 43 nm.

3.2. Morphological Analysis

The pure TiO_2 formed by employing the traditional sol-gel practice are revealed to be agglomerated in the transmission electron microscopy (TEM) in Figure 4a. In certain regions, some uniformly sized TiO_2 nanoparticles are present. The TEM picture displayed in Figure 4b is that of commercial TiO_2 (P25 Degussa). The P25 Degussa TiO_2 is free from agglomeration and has well-defined spherical morphology which will influence the proficiency of the pelargonidin-sensitized DSSCs.

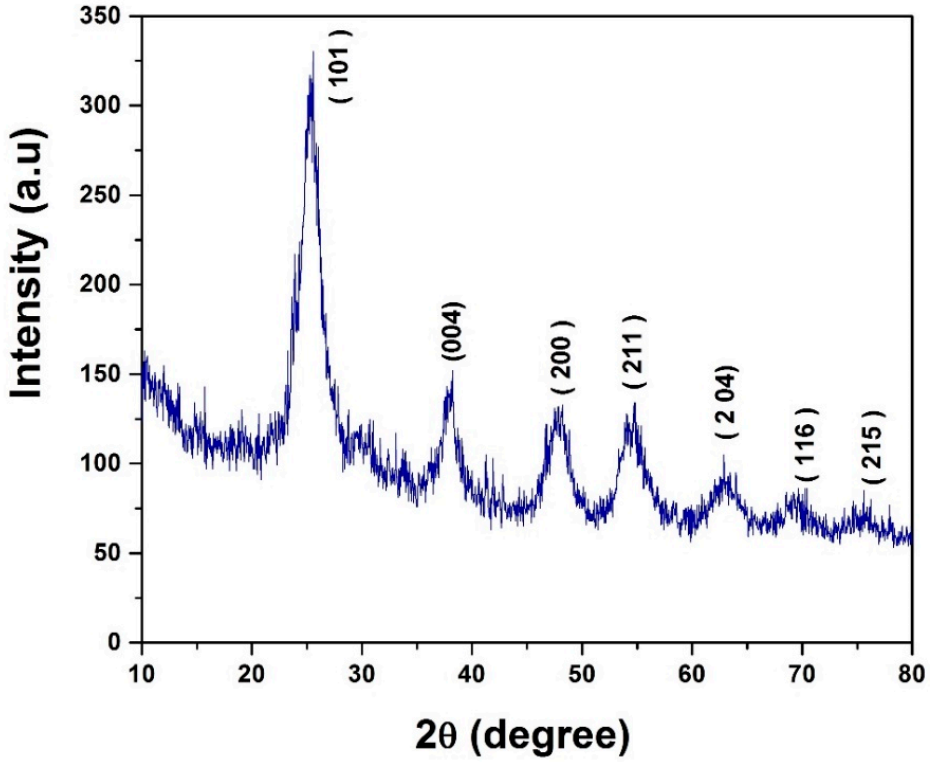

Figure 3. PXRD pattern of pure TiO_2 nanoparticles.

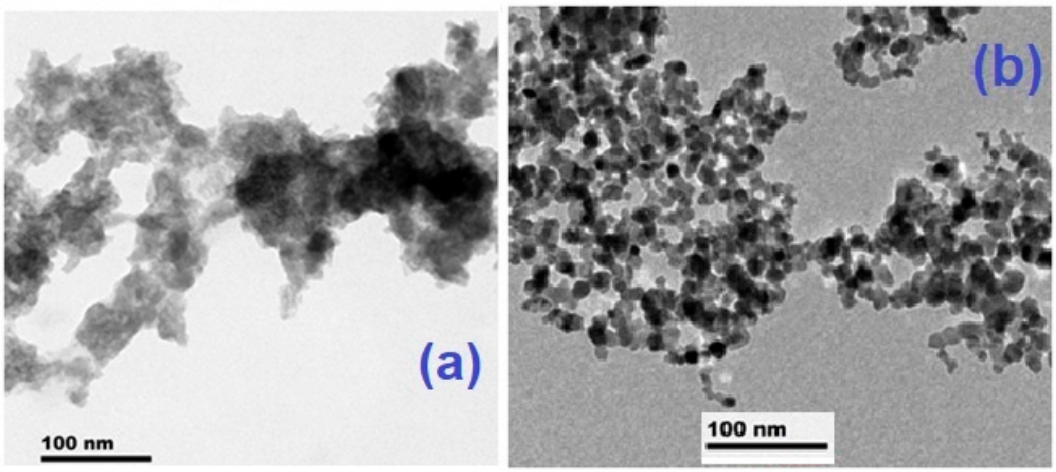

Figure 4. TEM images of pure TiO_2 by sol-gel process (**a**) and commercial P25 Degussa TiO_2 (**b**).

3.3. IR Vibrational Symmetry Analysis

The DFT/ B3LYP@ 6-311++G (d, p) was employed to compute vibrational spectra of molecules in both their ground and excited levels. The program can predict spectral frequencies and intensities as well as the molecular dislocations that it experiences during normal modes of vibration. A Gaussian broadening function can be used to create the spectra from a set of frequencies and intensities, as shown in Equation (1) [23].

$$I(\vartheta) = \sum_{k}^{N} \left(\frac{A_k}{\sqrt{2\pi\sigma}}\right) exp\left[\frac{-(\vartheta - \vartheta_o)^2}{2\sigma^2}\right] \quad (1)$$

The calculated intensity of each band for each of the N vibrational modes is given by Akin km/mol. Figure 5 shows observed FTIR spectra for PGN. For the wavelength

range of 4000–400 cm^{-1}, a thorough analysis of the infrared spectra of PGN-substituted derivatives in the solid and solution has been reported [24–26]. Table 1 lists the vibrational spectra of the compound prepared for this study. The vibrational assignments were calculated using crystal maker software. Wagging frequencies are in the neighborhood of 519 cm^{-1} with a second component of frequency around 809 cm^{-1} and a third set of scissoring at approximately 1329 cm^{-1}. The strong bands appearing in the spectrum at about 2117–3954 cm^{-1} are typical of C-H symmetric and asymmetric stretching. The band observed at 2117.24 cm^{-1} is due to C-H stretching with a strong peak. These assignments agree with the spectral work results for a compound that is present in solid form as a strongly hydrogen-bonded acid. Due to the aromatic C-C-C stretching vibrations, aromatic compounds frequently display numerous weak bands at 1948.56 cm^{-1} and 2467.12 cm^{-1}.

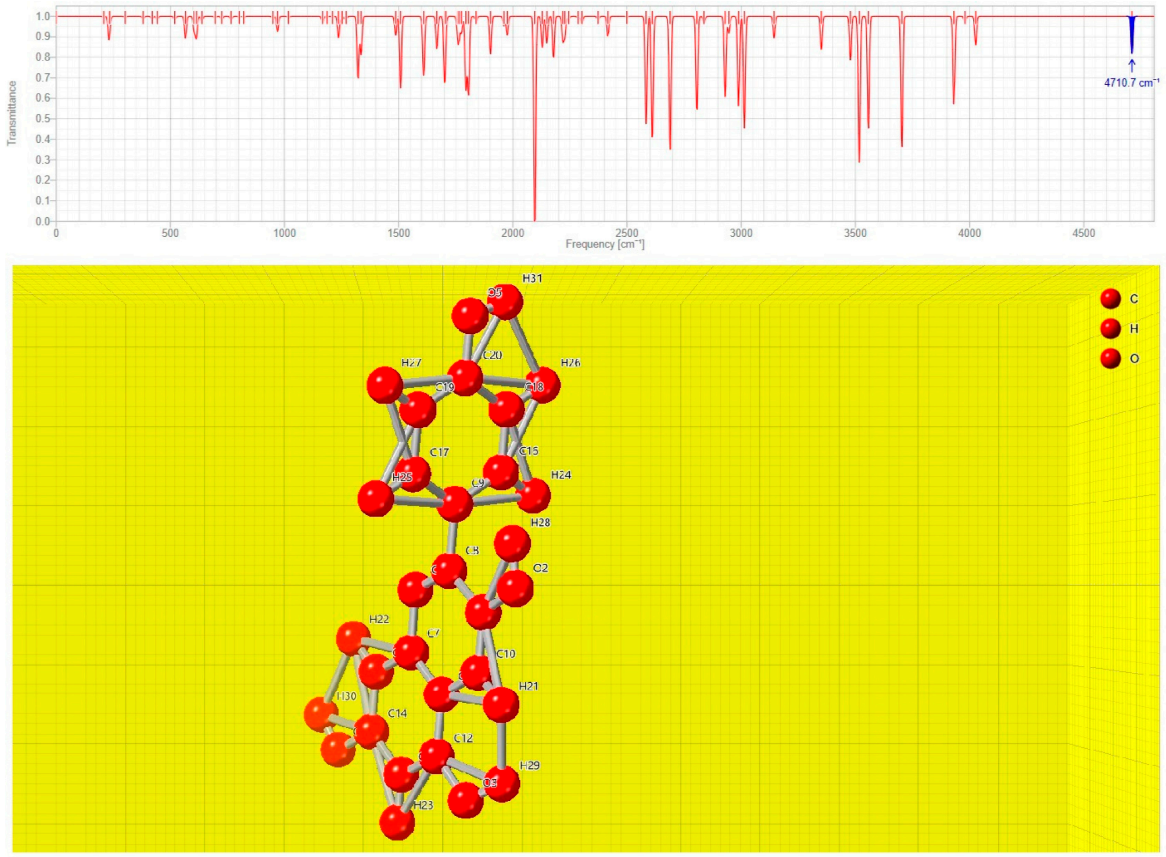

Figure 5. Computed FTIR symmetrical spectra for PGN.

Table 1. Physicochemical properties of PGN.

Physicochemical Properties	
Formula	$C_{15}H_{11}O_5+$
Molecular weight	271.24 g/mol
Num. heavy atoms	20
Num. aromatic heavy atoms	16
Fraction Csp3	0.00
Num. rotatable bonds	1
Num. H-bond acceptors	5
Num. H-bond donors	4
Molar refractivity	74.15
TPSA	94.06 $Å^2$
Energy	542.416 kJ/mol
Dipole moment	2.072D

3.4. Physicochemical & Electronic Parameter Computation

The inherent physical and chemical qualities of a substance are its physicochemical properties. These include things like flammability, density, volatility, water solubility, boiling point, etc. The physicochemical properties of PGN are presented in Table 1.

Frontier molecular orbital (FMO) energies were calculated as I = $-E_H$ and A = $-E_L$, according to Koopmans, where quantify ionization potential is I and electron affinity is A. Global hardness factor (η) = $1/2(E_L - E_H)$, chemical potential factor (μ) = $1/2(E_L + E_H)$, global electrophilicity factor (ω) = $\mu^2/2$ and global softness factor (ζ) = $1/\eta$ [27] were also calculated. Table 2 gives the calculated factors of α spin symmetry for I, A, ζ, η, μ and ω of PGN, which are +4.454 ev, +1.2383 ev, 0.6219 ev + 1.6078 ev, 2.8461 ev and 2.5596 ev, respectively. The β spin symmetries for I, A, ζ, η, μ and ω are +6.128 ev, +2.034 ev, 0.4884 ev, 2.047 ev, −4.081 ev and 4.068 ev respectively.

Table 2. Electronic parameters of PGN.

Electronic Parameters	**B3LYP/6-311G++(d, p) in GAS Phase PGN**		
Spin symmetry doublet	(α)		(β)
E_L (eV)	−1.2363		−2.034
E_H (eV)	−4.454		−6.128
E_L/E_H (eV)	0.278		0.3319
Ionization-potential factor (I) (eV)	+4.454		+6.128
Electron-affinity factor (A) (eV)	+1.2363		+2.034
Global hardness factor (η) (eV)	1.6078		2.047
Chemical potential factor (μ) (eV)	−2.8461		−4.081
Global electrophilicity factor (ω) (eV)	2.5596		4.068
Global softness factor (ζ) (eV^{-1})	0.6219		0.4884
Electronic spatial extent (a.u)		7604.76	
Nuclear repulsion energy (Hartrees)		1399.85	
Rotational constants (GHZ)	0.7756	0.152	0.133

3.5. FMO (Frontier Molecular Orbital) Analysis

The strength and stability of transition metal complexes, as well as the colors generated in solution, can be predicted using frontier molecular theory. The boundary molecular orbitals are HOMO and LUMO, which are implicated in chemical stability and lower reactivity in chemical processes [28,29]. The HOMO reflects the flexibility to offer the capacity to receive an electron; LUMO is an electron mediator [30]. This electron absorption transition occurs concurrently with the transition from lowest to first excited level and is principally represented by the excitation of an electron from the HOMO to the LUMO. The frontier orbital distance aids in distinguishing between the kinetic and chemical stability of molecular system reactivity [31]. Figure 6 depicts the atomic orbital composition, with positive and negative interactions characterized by red and green colors, respectively. PGN's HOMO, LUMO and frontier orbital gap energies of α and β spin symmetries are −4.454, −1.2383, −6.1282 and −2.034 eV, respectively.

3.6. UV–Visible Spectral Analysis

An ultimate photosensitizer absorbs all light photons up to the critical wavelength of 920 nm. Therefore, the preferred organic photosensitizers need to absorb higher energy photons in the solar spectrum. The electrons injected into TiO_2 were influenced by the attraction between the photosensitizer and its anchoring assemblage. There are several C=O and OH assemblies in the arrangements of atoms in the pelargonidin pigment that are skilled in anchoring to Ti. In addition, the prominent light photon absorption range of pelargonidin makes it a potential organic photosensitizer for DSSCs. The UV–vis spectra of pelargonidin-sensitized sol-gel-derived TiO_2 and Degussa TiO_2 nanoparticles are depicted

in Figure 7. The visible light absorption of TiO_2 was enhanced owing to the pelargonidin colorant, and the cutoff wavelength was 368 nm for sol-gel-derived TiO_2 and 392 nm for Degussa TiO_2. The TiO_2's band-gap energy was determined using cutoff wavelength (λ) with the equation Eg = h C/λc [Eg = 1239.8/λ eV (λ in nm)]. The band gaps of sol-gel-derived TiO_2 and Degussa TiO_2 were calculated as 3. 36 eV and 3. 16 eV respectively. This variation in Eg will influence the efficiency of the result.

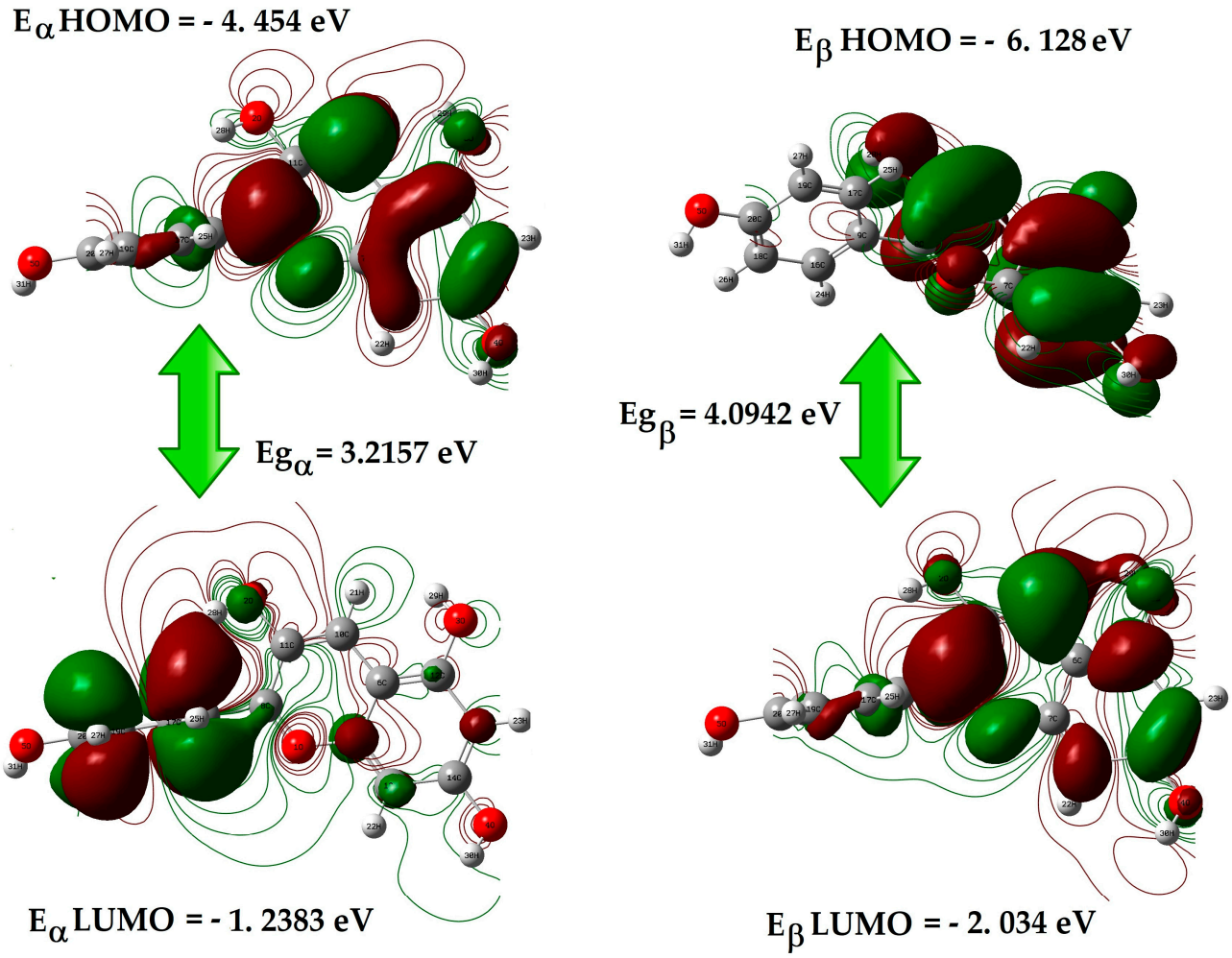

Figure 6. DFT/B3LYP/6–31G (d, p) 3D visualization of FMO orbitals in doublet α & β spin symmetry transition levels (HOMO–LUMO). (**a**) doublet α spin (**b**) doublet β spin.

3.7. Molecular Electrostatic Potential Map

The MESP surface, as shown in Figure 8, is very well suited for distinguishing one molecule from another via this potential and is highly valuable for determining the optimal places for electrophilic (negative region) and nucleophilic (positive region) reactions [32]. The levels of charge dispersion at the surface are embodied by the colors red, orange, yellow, green and blue. The color codes for these maps in the identified compound symmetry range from $-2.427e^{-2}$ (deepest red) to $+2.427e^{-2}$ (deepest blue), with blue denoting the most acceptor-positive or electron-rich region, and red denoting the most oxidized form or electron-poor region. The five oxygen atoms, which operate as electron donors, are clearly the most electronegative component of PGN molecule.

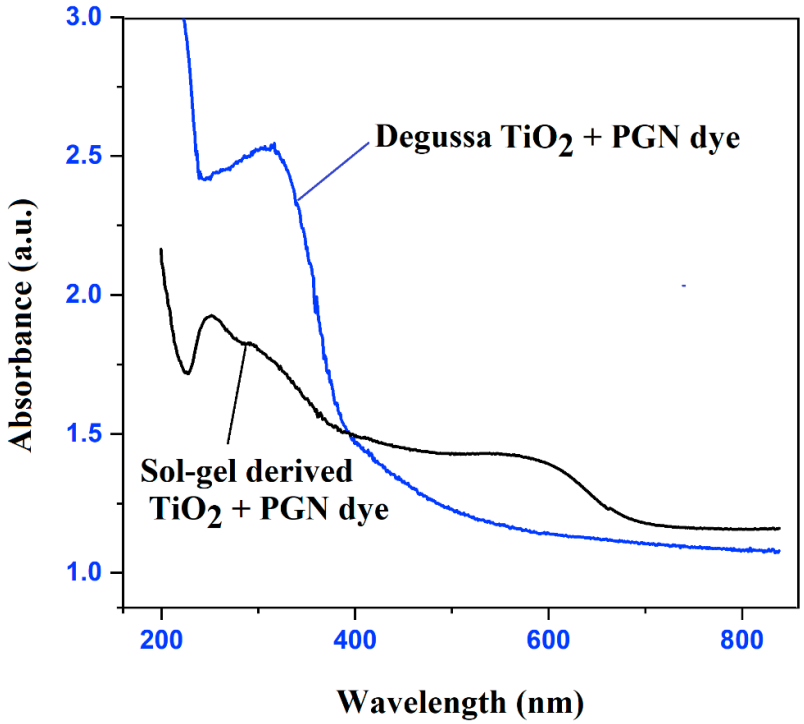

Figure 7. UV–Vis spectra of pelargonidin-sensitized sol-gel-derived TiO_2 and Degussa TiO_2.

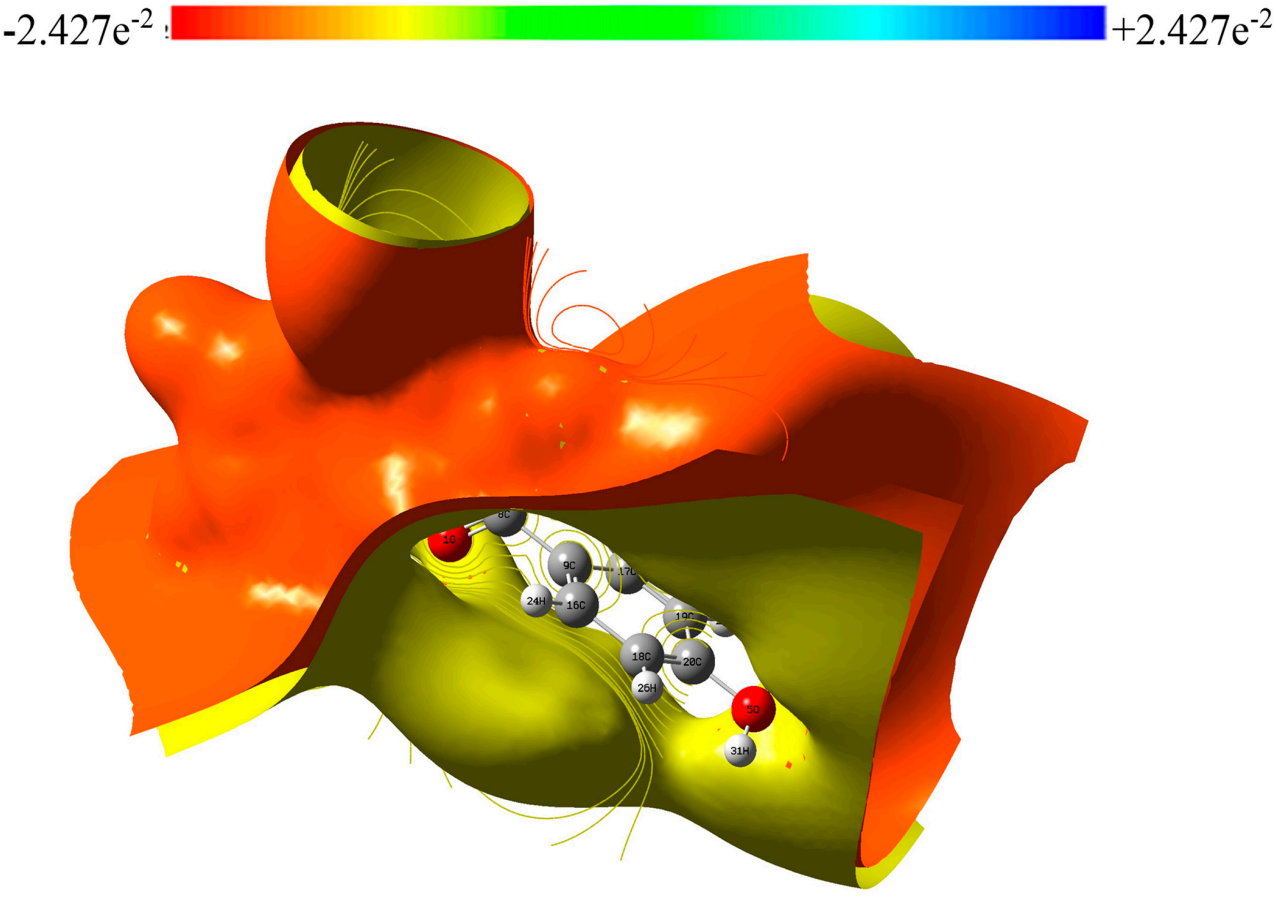

Figure 8. Potential distribution mapping of studied PGN.

3.8. IPCE Analysis

The incident photon to current conversion efficiency (IPCE) is very useful in evaluating the performance of solar cells. This measures the efficiency of incident photons converted into photocurrent flowing between the working and counter electrodes. The natural dye extracted from Tectona grandis seeds containing pelargonidin pigment as an acceptor exhibited stronger solar cell response in the 300–500 nm spectral region. The external quantum efficiency at any wavelength λ is [33,34]:

$$\text{IPCE\% } (\lambda) = 1240 \times \text{JSC Pin } \lambda$$

The observed quantum efficiency at the wavelength of 411 nm is 28%. The IPCE response of the pelargonidin photosensitizer is depicted in Figure 9.

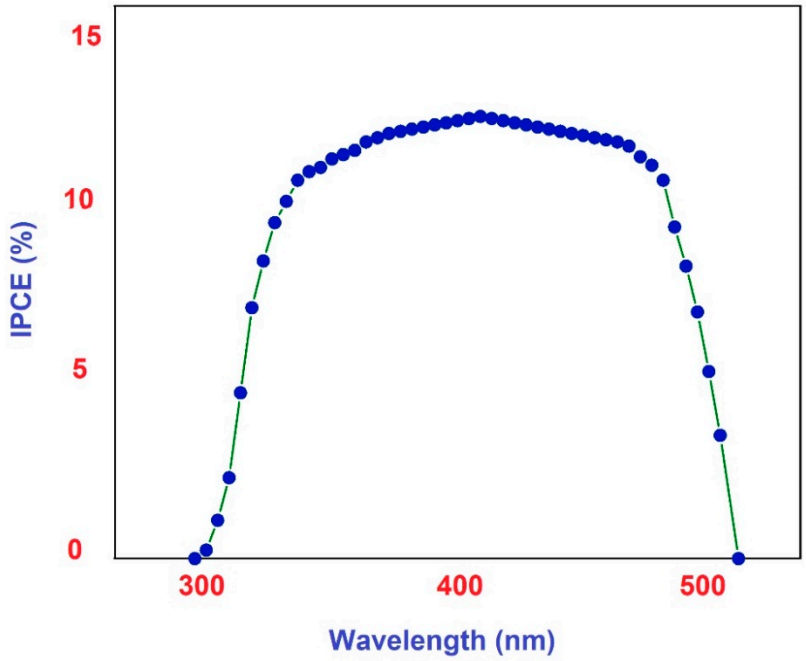

Figure 9. IPCE response of pelargonidin photosensitizer extracted from Tectona grandis seeds.

3.9. Efficiency Studies

The current-voltage characteristics of conventional sol-gel-prepared and P25 Degussa TiO_2-based DSSCs in Figure 10 show the values of J_{sc} as 2 $mAcm^{-2}$ and 4.9 $mAcm^{-2}$, and V_{oc} as 0.42 V and 0.55 V, respectively. Their fill factors are 68% and 61.6%, respectively. The light-to-electron conversion efficiency (η) of pure TiO_2-based DSSC was 0.68% and that of commercial P25 Degussa TiO_2-based DSSC was 1.18%. The Isc and η were found to be higher for P25 TiO_2-based DSSC than for synthesized TiO_2-based DSSC. This is attributed to more dye adsorption, superior morphology, abridged agglomeration and fewer colorant aggregations in commercial TiO_2 nanomaterials. Therefore, the pelargonidin photosensitizer extracted from Tectona grandis seeds is an operative photosensitizer for generating DSSCs with improved proficiency.

The relation shown below was used to get the total energy conversion efficiency:

$$\eta = (J_{sc} \times V_{oc} \times FF)/P_{in}$$

where P_{in} stands for the photon's energy at impact. The relation shown below was used to find the fill factor (FF):

$$FF = (J_{max} \times V_{max})/(J_{sc} \times V_{oc})$$

where J_{sc} is photocurrent density and V_{oc} is open-circuit voltage. J_{max} and V_{max} stand for the maximum current density and voltage, respectively. The solar parameters are given in Table 3.

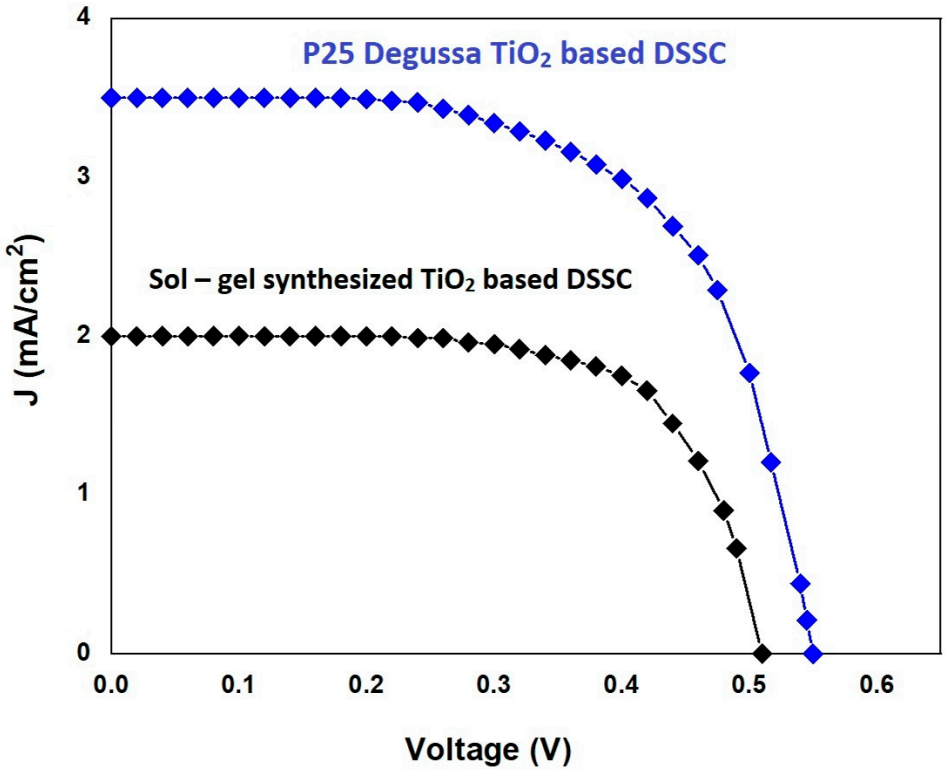

Figure 10. Current-voltage characteristics of sol-gel-synthesized TiO_2 and P25 Degussa TiO_2-based DSSC sensitized by pelargonidin natural colorant.

Table 3. Solar cell parameters.

Semi-Conductor	J_{sc} mAcm^{-2}	V_{oc} V	J_{max} mAcm^{-2}	V_{max} V	Fill Factor %	Efficiency η %
TiO_2 by sol-gel process (best cell)	2	0.42	1.65	0.34	68	0.68
TiO_2 by sol-gel process (test cell 1)	1.64	0.61	1.34	0.5	66.97	0.67
TiO_2 by sol-gel process (test cell 2)	1.95	0.49	1.55	0.39	63.27	0.6
P25 Degussa TiO_2 (best cell)	4.9	0.55	4.1	0.4	61.6	1.18
P25 Degussa TiO_2 (test cell 1)	3.3	0.49	2.72	0.40	67.26	1.1
P25 Degussa TiO_2 (test cell 2)	2.99	0.5	2.44	0.41	66.92	1

4. Conclusions

The structure of the organic colorant pelargonidin is validated by comprehensive UV–vis spectra and DFT data. The crystal is clear in the visible range of its spectrum, according to TD-DFT tests. The optical energy gap (DOS spectra and HOMO–LUMO), chemical reactivity (GCRD) and charge distribution all show the importance in electron density and MEP plots. The UV–Vis optical research confirms the molecule's hyper-conjugative interactions and stability. According to the experimental and computational investigation, this material possesses all of the needed properties for application in optical devices. Such behavior suggests that PGN will be the next diamond replacement, owing to its high thermal conductivity and refractive index but low hardness. PGN has emerged as a possible option for future photovoltaic devices. Hence, it can be adopted for better photosensitizer adsorption, amended morphology, abridged agglomeration, less dye aggregation and

upgraded efficacy. The pelargonidin-sensitized, synthesized, commercial P25 TiO_2-created dye-sensitized solar cells exhibited capable solar light energy-to-photon conversion proficiencies of 0.68% and 1.18%, correspondingly. The P25 Degussa TiO_2-based DSSC exhibited 57% higher proficiency in comparison to sol-gel yielded TiO_2-based DSSC.

Author Contributions: Conceptualization B.M. and A.S.; methodology, S.K.P.; software, P.P.; writing—review and editing, S.A.R.; validation, A.M.A.; formal analysis, A.K.U.; investigation, S.A.R. and A.S.; writing—original draft preparation, S.A.R. and A.S.; writing—review and editing, B.M. and A.S.; supervision, B.M. and A.S. All authors have read and agreed to the published version of the manuscript.

Funding: This research received no external funding.

Data Availability Statement: Not applicable.

Conflicts of Interest: The authors declare no conflict of interest.

References

1. Gojznikar, J.; Zdravković, B.; Vidak, M.; Leskošek, B.; Ferk, P. TiO_2 Nanoparticles and Their Effects on Eukaryotic Cells: A Double-Edged Sword. *Int. J. Mol. Sci.* **2022**, *23*, 12353. [CrossRef] [PubMed]
2. Shanmugama, V.; Manoharan, S.; Sharafalia, A.; Anandan, S.; Murugan, R. Green grasses as light harvesters in dye sensitized solar cells, Spectrochim. *Acta A Mol. Biomol. Spectrosc.* **2015**, *135*, 947–952. [CrossRef]
3. Chalkias, D.A.; Charalampopoulos, C.; Aivali, S.; Andreopoulou, A.K.; Karavioti, A.; Stathatos, E. A Di-Carbazole-Based Dye as a Potential Sensitizer for Greenhouse-Integrated Dye-Sensitized Solar Cells. *Energies* **2021**, *14*, 1159. [CrossRef]
4. Tecush Mohammadi, T.; Sharifi, S.; Ghayeb, Y.; Sharifi, T.; Momeni, M.M. Photoelectrochemical Water Splitting and H_2 Generation Enhancement Using an Effective Surface Modification of W-Doped TiO_2 Nanotubes (WT) with Co-Deposition of Transition Metal Ions. *Sustainability* **2022**, *14*, 13251. [CrossRef]
5. Konstantinova, E.; Zaitsev, V.; Marikutsa, A.; Ilin, A. Comparative Study: Catalytic Activity and Rhodamine Dye Luminescence at the Surface of TiO_2-Based Nano heterostructures. *Symmetry* **2021**, *13*, 1758. [CrossRef]
6. Liu, Y.; Chen, J.; Tian, Z.; Yao, J. Dye-Sensitized Solar Cell Based on TiO_2 Anode Thin Film with Three-Dimensional Web-like Structure. *Materials* **2022**, *15*, 5875. [CrossRef] [PubMed]
7. Dragonetti, C.; Colombo, A. Recent Advances in Dye-Sensitized Solar Cells. *Molecules* **2021**, *26*, 2461. [CrossRef]
8. Sarrato, J.; Pinto, A.L.; Cruz, H.; Jordão, N.; Malta, G.; Branco, P.S.; Lima, J.C.; Branco, L.C. Effect of Iodide-Based Organic Salts and Ionic Liquid Additives in Dye-Sensitized Solar Cell Performance. *Nanomaterials* **2022**, *12*, 2988. [CrossRef]
9. Zaky, A.A.; Alhumade, H.; Yousri, D.; Fathy, A.; Rezk, H.; Givalou, L.; Falaras, P. Modeling and Optimization of Triple Diode Model of Dye-Sensitized Solar Panel Using Heterogeneous Marine Predators Algorithm. *Mathematics* **2022**, *10*, 3143. [CrossRef]
10. Chinchillas-Chinchillas, M.J.; Garrafa-Gálvez, H.E.; Orozco-Carmona, V.M.; Luque-Morales, P.A. Comparative Study of SnO_2 and ZnO Semiconductor Nanoparticles (Synthesized Using *Randia echinocarpa*) in the Photocatalytic Degradation of Organic Dyes. *Symmetry* **2022**, *14*, 1970. [CrossRef]
11. Ananth, S.; Arumanayagam, T.; Vivek, P.; Murugakoothan, P. Enhanced photovoltaic behavior of dye sensitized solar cells fabricated using pre dye treated titanium dioxide nanoparticles. *J. Mater. Sci. Mater. Electron.* **2016**, *27*, 146–153. [CrossRef]
12. Lupaş, A.A.; Cătaş, A. An Application of the Principle of Differential Subordination to Analytic Functions Involving Atangana–Baleanu Fractional Integral of Bessel Functions. *Symmetry* **2021**, *13*, 971. [CrossRef]
13. Ahmad, A.; Khan, S.; Khan, M.; Luque, R.; Alsaiari, M.J.M.A. Microwave Assisted Preparation of Barium Doped Titania (Ba/TiO_2) as Photoanode in Dye Sensitized Solar Cells. *Appl. Sci.* **2022**, *12*, 9280. [CrossRef]
14. Kang, H.S.; Kim, W.S.; Kshetri, Y.K.; Kim, H.S.; Kim, H.H. Enhancement of Efficiency of a TiO_2-$BiFeO_3$ Dye-Synthesized Solar Cell through Magnetization. *Materials* **2022**, *15*, 6367. [CrossRef]
15. Ananth, S.; Vivek, P.; Arumanayagam, T.; Murugakoothan, P. Pre dye treated titanium dioxide nanoparticles synthesized by modified sol–gel method for efficient dye-sensitized solar cells. *App. Phy. A* **2015**, *119*, 989–995. [CrossRef]
16. Cingolani, S.; Gallo, M.; Tanaka, K. Symmetric Ground States for Doubly Nonlocal Equations with Mass Constraint. *Symmetry* **2021**, *13*, 1199. [CrossRef]
17. Ndiaye, A.; Dioum, A.; Oprea, C.I.; Dumbrava, A.; Lungu, J.; Georgescu, A.; Moscalu, F.; Gîrţu, M.A.; Beye, A.C.; Youm, I.; et al. A Combined Experimental and Computational Study of Chrysanthemin as a Pigment for Dye-Sensitized Solar Cells. *Molecules* **2021**, *26*, 225. [CrossRef]
18. Holliman, P.J.; Mohsen, M.; Connell, A.; Kershaw, C.P.; Meza-Rojas, D.; Jones, E.W.; Geatches, D.; Sen, K.; Hsiao, Y.W. Double Linker Triphenylamine Dyes for Dye-Sensitized Solar Cells. *Energies* **2020**, *13*, 4637. [CrossRef]
19. Elegbeleye, I.F.; Maluta, N.E.; Maphanga, R.R. Density Functional Theory Study of Optical and Electronic Properties of $(TiO_2)_{n=5,8,68}$ Clusters for Application in Solar Cells. *Molecules* **2021**, *26*, 955. [CrossRef]

20. Frisch, M.J.; Trucks, G.W.; Schlegel, H.B.; Scuseria, G.E.; Robb, M.A.; Cheeseman, J.R.; Scalmani, G.; Barone, V.; Mennucci, B.; Petersson, G.A.; et al. Theoretical Study of 5-HTP. Potential New Drug Resulting from the Complexation of 5-HTP with ATP. *Comp. Chem.* **2013**, *1*, 1–5.
21. O'boyle, N.M.; Tenderholt, N.A.L.; Langner, K.M. A library for package-independent computational chemistry algorithms. *J. Comput. Chem.* **2008**, *29*, 839–845. [CrossRef] [PubMed]
22. Blaney, B.L.; Ewing, G.E. Van Der Waals Molecules. *Annu. Rev. Phys. Chem.* **1976**, *27*, 553–584. [CrossRef]
23. Franzen, S. Use of Periodic Boundary Conditions to Calculate Accurate β-Sheet Frequencies Using Density Functional Theory. *J. Phys. Chem. A* **2003**, *107*, 9898–9902. [CrossRef]
24. Howard-Lock, H.E.; Lock, C.J.L.; Martins, M.L. Amino acid/zwitterion equilibria II: Vibrational and NMR studies of substituted thiazolidine-4-carboxylic acids. *Can. J. Chem.* **1991**, *69*, 1721–1727. [CrossRef]
25. Howard-Lock, H.E.; Lock, C.J.L.; Martins, M.L.; Smalley, P.S.; Bell, R.A. Amino-acid zwitterion equilibria: Vibrational and nuclear magnetic resonance studies of methyl-substituted thiazolidine-4-carboxylic acids. *Can. J. Chem.* **1986**, *64*, 1215–1219. [CrossRef]
26. Howard-Lock, H.E.; Lock, C.J.L.; Smalley, P.S. The crystal structure of racemic$_{DL}$-penicillamine and a spectroscopic study of$_{D}$-(−)-penicillamine. *J. Chem. Crystallogr.* **1983**, *13*, 333–353. [CrossRef]
27. Suvitha, A.; El-Mansy, M.A.M.; Kothandan, G.; Steephen, A. Molecular Structure, ft-raman, ir, nlo, nbo, homo–lumo analysis, physicochemical descriptors, adme parameters, and pharmacokinetic bioactivity of 2,3,5,6-tetrachloro-p-benzoquinone. *J Struct Chem.* **2021**, *62*, 1339–1356. [CrossRef]
28. El-Mansy, M.A.; Suvitha, A.; Ibrahim, M. Quantum Chemical Studies on Structural, Spectroscopic, Thermochemistry, Photophysical and Bioactivity Properties of m-Cresol Purple Dye. *Biointerface Res. Appl. Chem.* **2021**, *12*, 1006–1021. [CrossRef]
29. Ebrahimi, H.P.; Hadi, J.S.; Almayah, A.A.; Bolandnazar, Z.; Swadi, A.G.; Ebrahimi, A. Metal-based biologically active azoles and β-lactams derived from sulfa drugs. *Bioorg. Med. Chem.* **2016**, *24*, 1121–1131. [CrossRef]
30. Suvitha, A.R.; Maharani, N.Y.; Karikkad, H.K.; Varun, K.C.; Steephen, A. Quantitative Experimental and Theoretical Research using the DFT Technique on the Structural, UV, Electronic, and FMO Properties of Gammaxene. *Biointerface Res. Appl. Chem.* **2021**, *6*, 14240–14250.
31. Bradha, M.; Balakrishnan, N.; Suvitha, A.; Arumanayagam, T.; Rekha, M.; Vivek, P.; Ajay, P.; Sangeetha, V.; Steephen, A. Experimental, computational analysis of Butein and Lanceoletin for natural dye-sensitized solar cells and stabilizing efficiency by IoT. *Environ. Dev. Sustain.* **2022**, *24*, 8807–8822. [CrossRef]
32. Hiremath, S.M.; Khemalapure, S.S.; Hiremath, C.S.; Patil, A.S.; Basanagouda, M. Quantum chemical computational and spectroscopic (IR, Raman, NMR, and UV) studies on the 5-(5-methoxy-benzofuran-3-ylmethyl)-3h-[1,3,4]oxadiazole-2-thione. *J. Mol. Struct.* **2020**, *1210*, 128041. [CrossRef]
33. Wang, G.; Guo, W.; Xu, D.; Liu, D.; Qin, M. Graphene Oxide Hybridised TiO_2 for Visible Light Photocatalytic Degradation of Phenol. *Symmetry* **2020**, *12*, 1420. [CrossRef]
34. Niu, S.; Yang, W.; Wei, H.; Danilov, M.; Rusetskyi, I.; Popat, K.C.; Wang, Y.; Kipper, M.J.; Belfiore, L.A.; Tang, J. Heterostructures of Cut Carbon Nanotube-Filled Array of TiO_2 Nanotubes for New Module of Photovoltaic Devices. *Nanomaterials* **2022**, *12*, 3604. [CrossRef] [PubMed]